Analysis of Coupled Inset Dielectric Guides Under LSE and LSM Polarization

Steve R. Pennock, *Member, IEEE,* Dragan M. Boškovič, *Member, IEEE,* and Tullio Rozzi, *Fellow, IEEE*

***Abstract*—The inset dielectric guide (IDG) represents an easy-to-fabricate alternative to image line that is also less sensitive to loss by radiation at discontinuities. Two IDG's geometries were analyzed, the so-called deep and shallow IDG structures, operating in the LSE and LSM polarization, respectively. The propagation constants of single and coupled symmetrical IDG's have been calculated as well as the coupling coefficients of coupled guides. The Transverse Resonance Diffraction (TRD) method with variational formulation was used. Measured values show very good agreement with predicted values for the propagation constants of coupled deep slot IDG's. This information is a prerequisite for the design of directional couplers in IDG.**

I. Introduction

THE INSET DIELECTRIC GUIDE (IDG) shown in Fig. 1(a), has been proposed [1] as an alternative media to the image [2], Fig. 1(b), and insular [3], Fig. 1(c), varieties of dielectric based waveguides. IDG possesses advantages over these guides in terms of its ability to guide energy around relatively sharp bends with low radiation loss [4] and simple manufacture. Sharp bends naturally arise in circuits as higher circuit densities are considered, and in terms of its manufacture, this simple structure could be lightweight and cheap to mass produce through the use of plastic moulding and spray metallization techniques. It has also been seen that thin dipoles placed on the dielectric surface can be used to produce low mismatch, low cross-polarization antennas in IDG [5]–[7].

The modes of the IDG structure shown in Fig. 1(a) are hybrid in general, having three electric and three magnetic components. However, the deep and shallow slot configurations give rise to a great simplification in analysis. In fact, for a deep slot, the E_y component is small and the fields are approximately LSE [7], [8], while in a shallow slot H_y is small and the LSM approximation becomes apparent [6], [7]. It is under the assumption of pure LSE and LSM polarization that the analysis in this paper is performed, and verified by comparison with experiment. Choosing LSE/LSM five component field description rather than full six field hybrid gives a useful reduction in the size of the final matrix, and consequently faster computation.

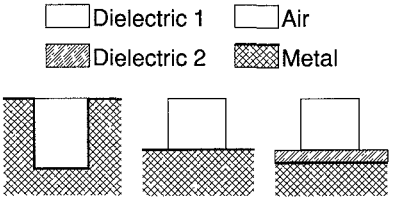

Fig. 1. Three types of dielectric surface waveguides. (a) Inset dielectric guide. (b) Image guide. (c) Insular guide.

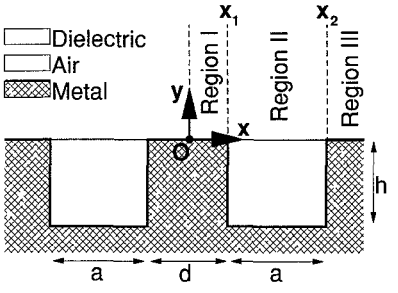

Fig. 2. Coupled symmetric IDG's.

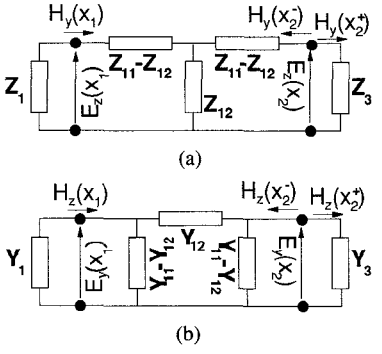

Fig. 3. Network representation of the integral operator equations under (a) LSE and (b) LSM polarizations.

In this paper we analyze the coupled IDG structure shown in Fig. 2 using the space domain Transverse Resonance Diffraction technique. This leads to the equivalent circuit representation in Fig. 3, where we have chosen to cast our analysis along the x direction. The obvious modifications of this cross-section, apart from the thickness of the spacing, are reductions in spacing height and the addition of a slot within the spacing. These modifications

Manuscript received April 15, 1991; revised December 4, 1991.

S. R. Pennock and D. M. Boskovic are with the University of Bath, School of Electronic and Electrical Engineering, Claverton Down, Bath, BA2 7AY, England.

T. Rozzi is with the Dipartmento di Electronica e Automatica, Universita degli Studi di Ancona, 60131 Ancona, Italy.

IEEE Log Number 9106770.

0018-9480/92$03.00 © 1992 IEEE

yield a method of controlling the coupling and dispersion characteristics of the lines.

We have limited ourselves to analyzing the coupling of identical IDG's in terms of even and odd excitation modes in this paper. However, the same TRD approach can be used for the analysis of non-identical IDG's, or even, for the characterization of multiple IDG arrays.

II. TRD Formulation and Network Modeling

The entire cross section is divided into three different regions as shown in Fig. 2, and the metal edges will be treated as discontinuities separating the regions. In each homogeneous part of the structure the propagation constants are linked by the relationship:

$$\epsilon_r k_o^2 = k_x^2 + k_y^2 + \beta^2 \tag{1}$$

where β is the z directed propagation constant, common for all regions, which is to be determined.

Considering the propagation in the x direction of the LSE$^{(y)}$ or LSM$^{(y)}$ modes, continuum modes are excited at each step discontinuity. In addition multiple reflection of the modes occur between the two steps. Thus region II can be no longer be represented by a few discrete transmission lines in any rigorous network representation. In fact, in order to analyze such a region, electric and magnetic walls are placed at $x = d/2$ and $x = d/2 + a$, in a manner analogous to the determination of the impedance or admittance parameters of a $2N$-port network by open and short circuit ports. Integral operators are then found relating the total E and H fields at the various ports under these "open" and "short circuit" conditions, and these are used to relate the total fields at each port to one another. Such an analysis follows closely the method described in [9], [10].

From such an analysis, we can express the transverse electric and magnetic fields on the first step as functions of the transverse electric and magnetic field on the second step and vice versa. Choosing a y directed field component as an independent variable, the above dependence can be expressed by means of a "two-port" Green's open-circuit impedance operator for the case of LSE polarization, or an admittance operator for the case of LSM polarization. This two-port circuit representation of region II will be terminated with impedance or admittance operators representing the driving point impedance, or admittance, of region I and III, thus completing the representation of the entire structure.

A. LSE Polarization

For the LSE$^{(y)}$ modes we use the H_y field as the unknown variable in our formulation, and the corresponding circuit representation is given in Fig. 3(a). The operator equations that link E_z and H_y at the two interfaces $x_1 = d/2$ and $x_2 = d/2 + a$ can be written in matrix form:

$$\begin{bmatrix} -E_z(x_1^-, y) \\ -E_z(x_2^+, y) \end{bmatrix} = \begin{bmatrix} -Z_{1e,o} & 0 \\ 0 & Z_3 \end{bmatrix} \cdot \begin{bmatrix} H_y(x_1^-, y) \\ H_y(x_2^+, y) \end{bmatrix} \tag{2}$$

and

$$\begin{bmatrix} E_z(x_1^+, y) \\ E_z(x_2^-, y) \end{bmatrix} = \begin{bmatrix} Z_{11} & Z_{12} \\ Z_{12} & Z_{11} \end{bmatrix} \cdot \begin{bmatrix} H_y(x_1^+, y) \\ H_y(x_2^-, y) \end{bmatrix} \tag{3}$$

where the dot product should be understood in the sense of operator multiplication. For example in (2) we have

$$E_z(x_1^-, y) = \int_0^\infty Z_{1e,o}(y, y') H_y(x_1, y')\, dy' = Z_{1e,o} \cdot H_y(x_1^-, y) \tag{4}$$

and the explicit form of the operator is derived in Section III.

Introducing the boundary conditions for electric and magnetic fields at the discontinuity planes in (2) and (3) results in

$$\begin{bmatrix} 0 \\ 0 \end{bmatrix} = \begin{bmatrix} Z_{11} - Z_{1e,o} & Z_{12} \\ Z_{12} & Z_{11} + Z_3 \end{bmatrix} \cdot \begin{bmatrix} H_y(x_1, y) \\ H_y(x_2, y) \end{bmatrix}. \tag{5}$$

This represents an operator formulation of the TRD dispersion equation which must be solved in order to obtain solutions for the propagation constants of the even and odd modes.

B. LSM Polarization

When considering shallow slot IDG's we approximate using a LSM$^{(y)}$ potential, and the TRD analysis is developed using E_y as the unknown. This determines admittance integral operators linking the E_y and H_z components at the discontinuity planes. The equivalent circuit representation for this LSM case is shown in Fig. 3(b) and the relevant matrix form of TRD dispersion equation is

$$\begin{bmatrix} 0 \\ 0 \end{bmatrix} = \begin{bmatrix} \mathcal{Y}_{11} - \mathcal{Y}_{1e,o} & \mathcal{Y}_{12} \\ \mathcal{Y}_{12} & \mathcal{Y}_{11} + \mathcal{Y}_3 \end{bmatrix} \cdot \begin{bmatrix} E_y(x_1, y) \\ E_y(x_2, y) \end{bmatrix} \tag{6}$$

III. Variational Formulation of Impedance Operators

We now derive the impedance operator equations under LSE polarization for each of the three regions separately. The LSM polarization admittance operators are given in Appendix I.

A. Region I

Magnetic wall at $x = 0$, or even mode

The expressions for the field components transverse to x under LSE polarization are

$$E_z(x, y) = \int_0^\infty d\rho\, V(\rho) \frac{k_{x\rho}}{\sqrt{k_{x\rho}^2 + \beta_e^2}} \sqrt{\frac{2}{\pi}} \cdot \cos(k_{x\rho} x) \sqrt{\frac{2}{\pi}} \sin(\rho y) \tag{7}$$

$$H_y(x, y) = \frac{1}{j\omega\mu_0} \int_0^\infty d\rho\ V(\rho) \sqrt{k_{x\rho}^2 + \beta_e^2} \sqrt{\frac{2}{\pi}} \cdot \sin(k_{x\rho} x) \sqrt{\frac{2}{\pi}} \sin(\rho y). \quad (8)$$

The elimination of the amplitude $V(\rho)$ gives an integral operator equation for the driving point impedance at the $x_1 = d/2$ plane with a magnetic wall at the $x = 0$ plane:

$$E_z(x_1^-, y) = \int_0^\infty dy' \int_0^\infty d\rho\ z_{e\rho} \cot\left(k_{x\rho} \frac{d}{2}\right) \sqrt{\frac{2}{\pi}} \cdot \sin(\rho y) \sqrt{\frac{2}{\pi}} \sin(\rho y') H_y(x_1^-, y) \quad (9)$$

$$E_z(x_1^-, y) = Z_{1e} \cdot H_y(x_1^-, y) \quad (10)$$

$$Z_{1,e} = \int_0^\infty d\rho\ z_{e\rho} \cot\left(k_{x\rho} \frac{d}{2}\right) \sqrt{\frac{2}{\pi}} \cdot \sin(\rho y) \sqrt{\frac{2}{\pi}} \sin(\rho y') \quad (11)$$

$$z_{e\rho} = j\omega\mu_0 \frac{k_{x\rho}}{k_{x\rho}^2 + \beta_e^2}. \quad (12)$$

Electric wall at $x = 0$, or odd mode

The transverse components, for the case when an electric wall is located at the $x = 0$ plane, have the form:

$$E_z(x, y) = \int_0^\infty d\rho\ V(\rho) \frac{k_{x\rho}}{\sqrt{k_{x\rho}^2 + \beta_o^2}} \sqrt{\frac{2}{\pi}} \cdot \sin(k_{x\rho} x) \sqrt{\frac{2}{\pi}} \sin(\rho y) \quad (13)$$

$$H_y(x, y) = \frac{-1}{j\omega\mu_0} \int_0^\infty d\rho\ V(\rho) \sqrt{k_{x\rho}^2 + \beta_o^2} \sqrt{\frac{2}{\pi}} \cdot \cos(k_{x\rho} x) \sqrt{\frac{2}{\pi}} \sin(\rho y). \quad (14)$$

The integral operator linking the two transverse field components in this case is

$$Z_{1,o} = -\int_0^\infty d\rho\ z_{o\rho} \tan\left(k_{x\rho} \frac{d}{2}\right) \sqrt{\frac{2}{\pi}} \sin(\rho y) \sqrt{\frac{2}{\pi}} \cdot \sin(\rho y') \quad (15)$$

$$z_{o\rho} = j\omega\mu_0 \frac{k_{x\rho}}{k_{x\rho}^2 + \beta_o^2}. \quad (16)$$

B. Region II

We now establish a relationship between the fields at $x_1 = d/2$ and $x_2 = a + d/2$, which describes the effect of the finite length of the slab waveguide between the steps. When a magnetic wall is placed at x_2 the transverse electric field $E_z(x_1^+, y)$ excited by $H_y(x_1^+, y)$ is

$$E_z(x_1^+, y) = Z_{11} \cdot H_y(x_1^+, y) \quad (17)$$

$$Z_{11} = \sum_{k=1}^{Nsw} z_k \cot(k_{xk} a) \Phi_{dk}(y) \Phi_{dk}(y') + \int_0^\infty d\rho\ z_\rho \cot(k_{x\rho} a) \Phi(\rho, y) \Phi(\rho, y') \quad (18)$$

$$z_k = -j\omega\mu_0 \frac{k_{xk}}{k_{xk}^2 + \beta_{e,o}^2}$$

$$z_\rho = -j\omega\mu_0 \frac{k_{x\rho}}{k_{x\rho}^2 + \beta_{e,o}^2} \quad (19)$$

where N_{sw} stands for total number of surface waves supported by the grounded dielectric slab. Expression (18) is the operator form of the driving point impedance of an open-circuit stub. Moreover, under the same boundary conditions, we have

$$E_z(x_1^+, y) = Z_{12} \cdot H_y(x_2^-, y) \quad (20)$$

where Z_{12} is determined from Z_{11} by replacing the cot function with the csc function.

When a magnetic wall is placed at x_1, $H_y(x_1^+, y)$ is zero, and then symmetry and reciprocity give

$$E_z(x_2^-, y) = Z_{11} \cdot H_y(x_2^-, y) \quad (21)$$

$$E_z(x_2^-, y) = Z_{12} \cdot H_y(x_1^+, y). \quad (22)$$

The function $\Phi_k(y)$ and $\Phi_\rho(y, \rho)$ are the well known scalar mode functions for the TE surface continuous waves of a grounded slab guide [5].

C. Region III

This region was treated as half open space region, and the field expressions are

$$E_z(x, y) = \int_0^\infty d\rho\ V(\rho) \frac{jk_{x\rho}}{\sqrt{k_{x\rho}^2 + \beta_{e,o}^2}} \frac{1}{\sqrt{2\pi}} \cdot \exp^{-jk_{x\rho}x} \sqrt{\frac{2}{\pi}} \sin(\rho y) \quad (23)$$

$$H_y(x, y) = -\frac{1}{j\omega\mu_0} \int_0^\infty d\rho\ V(\rho) \sqrt{k_{x\rho}^2 + \beta_{e,o}^2} \frac{1}{\sqrt{2\pi}} \cdot \exp^{-jk_{x\rho}x} \sqrt{\frac{2}{\pi}} \sin(\rho y) \quad (24)$$

Finding the inverse transformation of (24) and substituting into (23) gives an integral equation for the driving point impedance at the plane $x_2 = d/2 + a$:

$$Z_3 = \int_0^\infty d\rho\, z_\rho \sqrt{\frac{2}{\pi}} \sin(\rho y) \sqrt{\frac{2}{\pi}} \sin(\rho y') \quad (25)$$

$$z_\rho = \omega\mu_0 \frac{k_{x\rho}}{k_{x\rho}^2 + \beta_{e,o}^2}. \quad (26)$$

IV. Discretization and Choice of Basis Functions

In order to solve the dispersion operator equations (5) and (6), they must first be discretized. The equation is discretized by transforming it into a function space which is spanned by the set of functions used to expand the unknown fields. As the same numerical approach is used for discretizing both operator equations, the procedure used will be described using a unified notation. In order to do so, the operator equations are written as

$$\begin{bmatrix} \mathbf{0} \\ \mathbf{0} \end{bmatrix} = \begin{bmatrix} \mathbf{\Lambda}_{11} - \mathbf{\Lambda}_{1e,o} & \mathbf{\Lambda}_{12} \\ \mathbf{\Lambda}_{12} & \mathbf{\Lambda}_{11} + \mathbf{\Lambda}_3 \end{bmatrix} \cdot \begin{bmatrix} \boldsymbol{X}_1 \\ \boldsymbol{X}_2 \end{bmatrix} \quad (27)$$

where $\Lambda = Z$ in the LSE case and $\Lambda = \mathcal{Y}$ in the LSM case. The above equation has nontrivial solutions when

$$\det \begin{bmatrix} \mathbf{\Lambda}_{11} - \mathbf{\Lambda}_{1e,o} & \mathbf{\Lambda}_{12} \\ \mathbf{\Lambda}_{12} & \mathbf{\Lambda}_{11} + \mathbf{\Lambda}_3 \end{bmatrix} = 0. \quad (28)$$

This is the dispersion equation which is solved to determine even and odd mode propagation constants.

The approach used here was the Ritz–Galerkin method, where the unknown field functions are written in terms of a suitable set of basis functions. The problem has been formulated so that only one set of basis functions is used for both of the singular unknown field quantities, which improves both efficiency and accuracy. The unknown field possesses singularities at the 90° metal edges which occur in the IDG structure, of the order $r^{-1/3}$ where r is a distance from the corner [11]. Thus, an appropriate complete set of basis functions is provided by the generalized Laguerre polynomial, whose weight function fits the required singularity at the metal corners and which are expressed mathematically as

$$\mathfrak{L}_m(y) = \frac{1}{N_{m-1}} (y_o a)^{-1/2} \left(\frac{y}{y_o a}\right)^{-1/3} \cdot \exp^{-y/y_o a} L_{m-1}^{-1/3}\left(\frac{y}{y_o a}\right) \quad (29)$$

with the orthogonality relationship [12]:

$$\int_0^\infty \mathfrak{L}_m(y) \times L_{n-1}^{-1/3}\left(\frac{y}{y_o a}\right) dy = N_{m-1}\, \delta_{mn} \quad (30)$$

and normalization constant N_{m-1} given as

$$N_{m-1}^2 = \frac{\Gamma(m - 1/3)}{(m-1)!}. \quad (31)$$

The arbitrary scale parameter y_o can be adjusted so as to optimize convergence. To determine y_o we define an error function (32) which represents a measure of completeness of the basis function set for the discrete modes of a grounded slab dielectric waveguide:

$$f_{\text{error}}(y_o, N, \text{freq}, \epsilon_r, a, h) = \sum_{k=1}^{N_{sw}} \left(\|\Phi_{dk}(y)\|^2 - \sum_{m=1}^{N} \|\langle \Phi_{dk}(y), \mathfrak{L}_m(y)\rangle\|^2 \right). \quad (32)$$

For the geometry considered here, we can expand the modes of region I and region II on the first discontinuity plane, and modes of region II and region III on the second discontinuity plane, using the same basis functions. The transformer coefficients are given by

$$P_{m\rho} = \langle \Upsilon_{1,3}, \mathfrak{L}_m \rangle = \int_0^\infty dy\, \Upsilon_{1,3}(\rho, y)\, \mathfrak{L}_m(y) \quad (33)$$

$$A_{mk} = \langle \Upsilon_{2k}, \mathfrak{L}_m \rangle = \int_0^\infty dy\, \Upsilon_{2k}(y)\, \mathfrak{L}_m(y) \quad (34)$$

$$A_{m\rho} = \langle \Upsilon_2, \mathfrak{L}_m \rangle = \int_0^\infty dy\, \Upsilon_2(\rho, y)\, \mathfrak{L}_m(y) \quad (35)$$

where Υ is the scalar mode function of the region considered. Using (29) as a basis set the rectangular $N_{sw} \times N$ transformer matrix, $\boldsymbol{A}$, for discrete modes and $\boldsymbol{P}(\rho)$ and $\boldsymbol{A}(\rho)$, $1 \times N$ vectors for the continuous mode are established. The discretized operators are defined as

$$\mathbf{\Lambda}_{1,3} = \int_0^\infty d\rho\, \boldsymbol{P}^T(\rho) \lambda_{\rho 1,3} \boldsymbol{P}(\rho) \quad (36)$$

$$\mathbf{\Lambda}_{11,12} = \sum_{n=1}^{N_{sw}} \boldsymbol{A}^T \lambda_{k11,12} \boldsymbol{A} + \int_0^\infty d\rho\, \boldsymbol{A}^T(\rho) \lambda_{\rho 11,12} \boldsymbol{A}(\rho) \quad (37)$$

The numerical complexity of the semi-infinite integrals is increased by the fact that λ_ρ possesses a singularity for $\rho = k_0$. Thus the integration comprises a principal value estimation.

The resulting $N \times N$ matrices can be interpreted as impedances or admittances of an ordinary N port, which approximates the field problem in the Ritz–Galerkin sense and is amenable to ordinary network analysis.

V. Numerical and Experimental Results

A. Numerical Results

The optimum value of y_o was determined by searching for the global minimum of (32). This scale factor is important in terms of achieving fast convergence and high accuracy and example values for two different IDG geometries are given in Table I. By introducing y_o into the basis set only 4 to 5 terms in expansion were sufficient in the cases examined here. The optimization of y_o requires

TABLE I
COMPUTED VALUES FOR SCALE CONSTANTS UNDER LSE AND LSM POLARIZATION FOR DEEP AND SHALLOW IDG GEOMETRY (NUMBER OF BASIS FUNCTION = 5)

Freq. GHz	8	9	10	11	12
y_0 LSE deep	0.627	0.492	0.407	0.349	0.306
y_0 LSE shallow	0.906	0.447	0.301	0.229	0.186
y_0 LSM shallow	0.213	0.179	0.155	0.137	0.122

TABLE II
CONVERGENCE TEST FOR THE LSE_{01} MODE PROPAGATION CONSTANT IN A DEEP SLOT IDG, AND COMPARISON WITH MEASURED DATA (THE IDG IS FILLED WITH PTFE AND OF DIMENSIONS 10.16 mm × 15.24 mm)

Freq. GHz	7	9	11	13
$N = 3$	162.32	224.56	285.77	346.34
$N = 4$	163.54	227.65	291.91	355.13
$N = 5$	163.50	228.28	293.18	357.15
Meas.	160.1	230.3	293.9	357.4

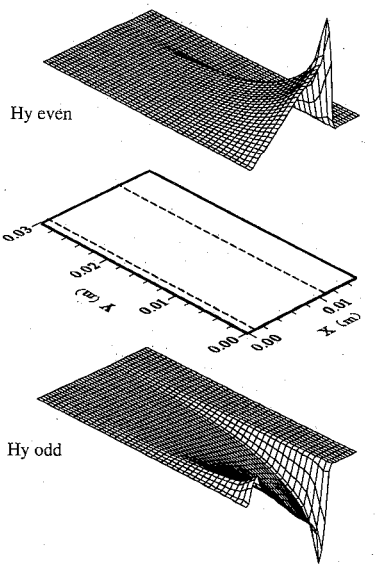

Fig. 4. H_y field pattern for odd and even mode of coupled deep IDG's. Guide dimensions are 10.16 × 15.24 mm filled with PTFE and separated by 2.0 mm. The dashed lines mark interfaces between the three regions depicted in Fig. 2.

little CPU time, and typically took 0.5 s of CPU time on a HP9000-845 machine.

The convergence behavior of the analysis is shown in Table II for several frequencies in the monomode operating range of a single IDG line. These tests show that solutions are stable to less than 0.5% using only five basis functions in the expansion set for the unknown field. Such a degree of accuracy does probably exceed the precision to which the permittivity of the IDG filling is known, and so might be thought of as being excessive. However, the properties of coupled IDG lines rely on the relatively small difference between the phase constants of the even and odd modes. Consequently, high accuracy is needed to evaluate this difference and we have used five or six functions in the coupled line computations shown in this paper. The CPU time taken to evaluate each phase constant was about 1.5 min on our HP9000-845, most of which is caused by evaluating the determinant function about 12 times.

B. Computation of Field Components

Having solved the dispersion equation (27) for even and odd modes, the phase constants $\beta_{e,o}$ for both modes are known and the amplitude coefficients for the basis set are found by placing the phase constant back into operators and solving the eigenvalue equation:

$$-\begin{vmatrix} A \\ A \end{vmatrix} = \begin{vmatrix} \Lambda_{11c} - \Lambda_{1e,o} & \Lambda_{12c} \\ \Lambda_{12c} & \Lambda_{11c} + \Lambda_3 \end{vmatrix} \cdot \begin{vmatrix} X_1 \\ X_2 \end{vmatrix} \quad (38)$$

The amplitude coefficients of the field amplitudes can then be evaluated enabling the field components to be calculated separately for all three regions. The 3-D plots for even and odd H_y in the air region over coupled IDG lines under LSE polarization are shown in Fig. 4. At the two discontinuity planes, the edge condition requires that x and y directed field components show singular behavior. From the plots it is apparent that edge influence is stronger on the second discontinuity plane. The presence of magnetic wall, for the even mode case, close to the slot edge strongly reduces the field spike.

C. Phase Constant Measurements

The phase constants of the coupled IDG lines were measured by terminating a length of coupled IDG lines at both ends and then introducing weak coupling magnetic loop probes near these ends. Power transmission through this structure shows resonant peaks when the interceding transmission path is an integral number of half wavelengths long, and so we can determine phase constants at discrete frequencies. Accuracy is improved by reducing the peak transmission magnitude, and this can be controlled through the separation between the probe and the IDG. In addition, probe orientation facilitates relatively independent excitation of even and odd symmetry modes, allowing discrimination between fundamental and higher order modes of the single lines and between even and odd modes of the coupled lines.

The deep IDG structures tested here have a slot width of 10.16 mm, a depth of 15.24 mm, and are filled with PTFE, while the shallow structures were 22.86 mm wide and 10.16 mm deep. Considering the deep slot IDG, the comparison between experiment, full six-field hybrid mode calculation [8], and our LSE approximation, is made in Fig. 5. While phase constant data is required to characterize signal propagation (e.g. coupling effects, delay etc.), we show the effective permittivity in order to make any differences between data more apparent. The difference between the LSE approximation and experimentally determined phase constant is greatest at frequencies approaching cut-off, and lies in the range of 1.3% to 0.5% of the theoretical value.

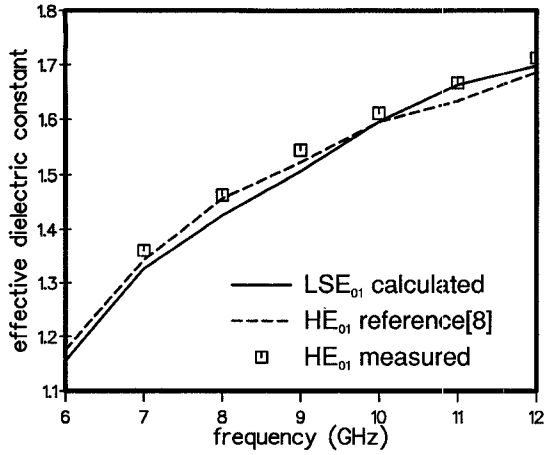

Fig. 5. Dispersion characteristic of single deep 10.16 × 15.24 mm IDG filled with PTFE.

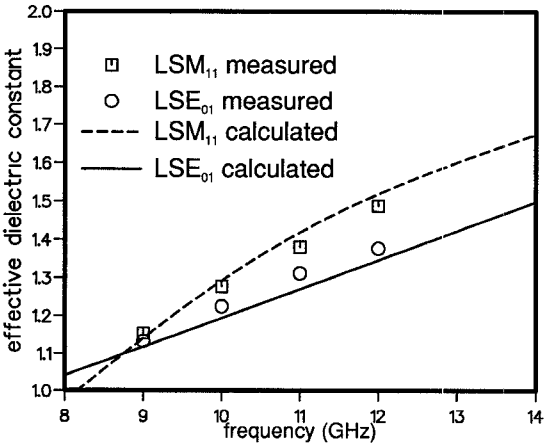

Fig. 6. Dispersion characteristic of single shallow 22.86 × 10.16 mm IDG filled with PTFE.

Fig. 6 shows the comparison between experiment and theory for a shallow slot guide for frequencies between 8 GHz and 14 GHz. LSM analysis of the structure shows the existence of an LSM_{11} mode, but by applying the LSE analysis we find two additional modes, the LSE_{01} and LSE_{02} modes. Experimental data show that the guide does indeed support two propagating modes in this frequency range. The difference in phase constant between experiment and calculation lies in the range 1.7%–0.75%. It has been suggested [8] that the LSM_{mn} modes can approximate the EH_{mn} hybrid modes, while the LSE_{mn} mode can approximate the HE_{mn} hybrid mode. As we can see from our data, this is a reasonable approach, allowing fairly accurate prediction of the phase constants and modal structure from the LSE/LSM analysis. Monomode operation of a shallow IDG can be achieved by making width/height ratio large enough, for the LSM_{11} to emerge as the fundamental mode of the structure.

Computed and measured data for the case of coupled lines with a separation of 0.47 mm are compared in Fig. 7, and agreement is very good for both the even and odd modes. Theoretical and measured phase constants differ by between 0.7% and 0.15%. The comparison for a separation of 1.7 mm is presented in Table III where the even and odd mode phase constants differ by between 3% and 0.7%. In using a five function basis we have kept the error between calculated and measured data between 0.3% and 0.08%, i.e., about one tenth of the difference in even and odd mode phase constants.

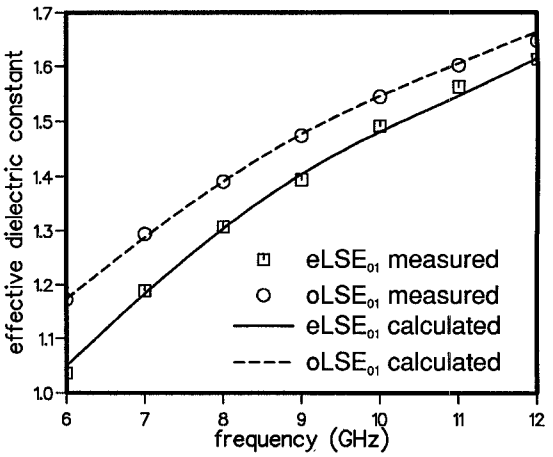

Fig. 7. Dispersion characteristic of deep coupled IDG's for both even(e) and odd(o) modes. Guide dimensions are 10.16 × 15.24 mm filled with PTFE and separate by 0.47 mm.

TABLE III
COMPUTED AND MEASURED VALUES FOR β OF COUPLED IDG'S DIMENSIONS 1.016 × 1.524, FILLED WITH PTFE AND SEPARATED BY d = 1.7 mm

Freq.	β_e^c	β_e^m	β_o^c	β_o^m
8	197.49	198.1	202.86	203.1
9	228.56	230.0	233.42	234.3
10	260.41	260.9	264.76	265.4
11	292.77	292.2	296.18	296.2
12	324.06	323.8	326.41	326.6

D. Coupling Effects

Using a dielectric taper inside the metal rectangular waveguide as a transition section into a single deep slot IDG, a return loss in the region of −20 dB is observed over the entire X band frequency range [8]. The characteristics of a 25 cm long coupled section with a separation of 1.7 mm were measured using an HP8510 network analyzer, with the remaining coupler ports matched. The coupled IDG section was seen to perform as a forward coupler with return loss and isolation better than −20 dB [13]. From these results, we can see that the coupler can be approximated very well by assuming perfect isolation and port matching, in which case the coupling can be calculated very simply from:

$$\|S_{13}\| = 10 \times \log\left(\sin^2\left(\frac{\beta_{\text{even}} - \beta_{\text{odd}}}{2} \times L\right)\right). \quad (39)$$

To examine the dependence of coupling on separation and of the filling material permittivity, we have plotted the coupling per coupled guide wavelength against guide separation in Fig. 8. The upper line designated IDG_1 is

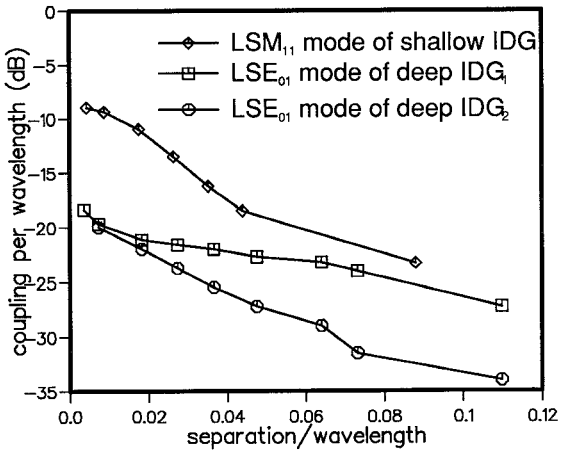

Fig. 8. Coupling characteristics for deep slot LSE_{01} mode and shallow slot LSM_{11} mode versus guide separation at 9 GHz. Dimensions for IDG_1 are 10.16 × 15.24 filled with PTFE ($\epsilon_r = 2.08$). Dimensions of IDG_2 were 3.24 × 4.86 mm and dielectric filling was $\epsilon_r = 10.8$. Shallow slot was PTFE filled and 22.86 × 10.16 mm.

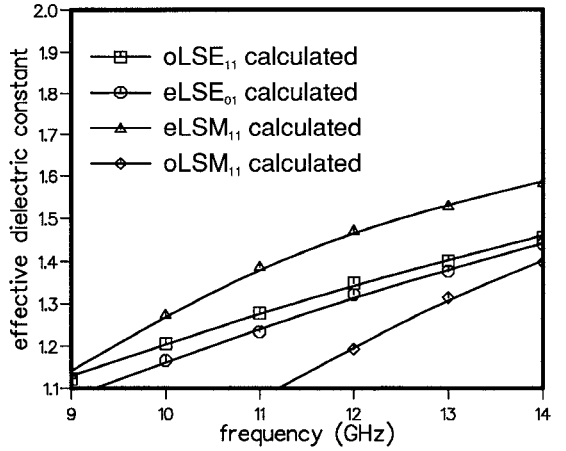

Fig. 9. Dispersion characteristics of coupled shallow 22.86 × 10.16 mm IDG filled with PTFE. Calculations are for both even(e) and odd(o) modes, and for both LSE and LSM polarizations.

for the PTFE filled guides we have considered so far, while IDG_2 refers to a guide filled with a higher permittivity material. This second example has a smaller cross section so that comparison is made for coupled lines with equal operating frequency bands. By this we mean that both structures have the same cut-off frequencies for the fundamental and first higher order pairs of modes, about 6 GHz and 14 GHz, respectively. Clearly the higher permittivity filling acts to concentrate the fields within the slot and reduce the coupling effect. Consequently, in applications where coupling is to be avoided, smaller IDG's filled with a high permittivity material should be used. Such an application might be the implementation of parallel sets of radiating dipoles in a two dimensional array antennas. The reduction in guide size facilitates the avoidance of grating lobes, while the coupling could be reduced to negligible levels, greatly simplifying analysis and design.

The dispersion characteristics for the LSM_{11} and LSE_{01} modes of 0.5 mm spaced shallow IDG's are presented in Fig. 9. The coupling is much greater for the LSM_{11} mode than for the LSE_{01} mode of the same shallow IDG. The coupling characteristic for the LSM_{11} mode is also shown in Fig. 8 for comparison with the deep slot data. Clearly for small guide separations the coupling is much stronger in the shallow slots, while for separations of $d \geq 0.08\,\lambda_g$ the coupling factors are quite similar.

VI. Conclusion

We have described the accurate analysis of coupled IDG's under LSE and LSM polarizations. The convergence of the analysis has been demonstrated to be good, typically needing only 5 terms to provide the 4 figure accuracy needed to describe coupling properly. Good agreement with experimentally measured data for the deep slot case has also been demonstrated. Some of the features of IDG directional couplers have been illustrated showing good isolation/directivity and port matching characteristics.

The analysis presented here can be applied to the design of directional couplers, coupled line bandpass filters and two dimensional array antennas in IDG. Consequently, power splitting and filtering operations can now be included in the same IDG circuit media as the antenna, thus providing a complete front end sub-assembly. Further work is being undertaken at present towards this aim.

Appendix I
Admittance Operators for LSM Polarization

A. Region I

Even mode

$$H_z(x_1^-, y) = \mathcal{Y}_{1e} \cdot E_y(x_1^-, y) \tag{40}$$

$$\mathcal{Y}_{1,e} = \int_0^\infty d\rho\, y_{e\rho} \tan\left(k_{x\rho}\frac{d}{2}\right)\sqrt{\frac{2}{\pi}} \cdot \cos(\rho y)\sqrt{\frac{2}{\pi}}\cos(\rho y') \tag{41}$$

Odd Mode

$$\mathcal{Y}_{1,o} = \int_0^\infty d\rho\, y_{o\rho} \tan\left(k_{x\rho}\frac{d}{2}\right) \cdot \sqrt{\frac{2}{\pi}}\sin(\rho y)\sqrt{\frac{2}{\pi}}\sin(\rho y') \tag{42}$$

where

$$y_{e,o\rho} = j\omega\epsilon\frac{k_{x\rho}}{k_{x\rho}^2 + \beta_{e,o}^2}. \tag{43}$$

B. Region II

When an electric wall is placed at $x_2 = a + d/2$ the transverse magnetic field $H_z(x_1^+, y)$ excited by $E_y(x_1^+, y)$ is

$$H_z(x_1^+, y) = \mathcal{Y}_{11} \cdot E_y(x_1^+, y)$$

$$\mathcal{Y}_{11} = \sum_{k=1}^{N_{sw}} y_k \cot(k_{xk}a)\Psi_{dk}(y)\Psi_{dk}(y') + \int_0^\infty d\rho\, y_\rho \cot(k_{x\rho}a)\Psi(\rho, y)\Psi(\rho, y') \tag{45}$$

$$y_{k,\rho} = -j\omega\epsilon \frac{k_{x(k,\rho)}}{k_{xk}^2 + \beta_{e,o}^2}. \tag{46}$$

This expression is the operator form of the driving point admittance of a short-circuit stub. Moreover, under the same boundary conditions, we have

$$H_z(x_1^+, y) = \mathcal{Y}_{12} \cdot E_y(x_2^-, y) \tag{47}$$

where $\mathcal{Y}_{12}$ is determined from (45) by replacing the cot function with csc function.

The two remaining parameters are determined, as in the LSE case, by the conditions of reciprocity and symmetry.

The functions $\Psi_k(y)$ and $\Psi_\rho(y, \rho)$ are the well-known expressions for the TM surface wave of grounded slab guide, [14].

C. Region III

$$\mathcal{Y}_3 = \int_0^\infty d\rho\, y_\rho \sqrt{\frac{2}{\pi}}\cos(\rho y)\sqrt{\frac{2}{\pi}}\cos(\rho y') \tag{48}$$

$$y_\rho = \omega\epsilon \frac{k_{x\rho}}{k_{x\rho}^2 + \beta_{e,o}^2}. \tag{49}$$

Appendix II

The coefficient $P_{m\rho}$ has been defined as

$$P_{m\rho} = \int_0^\infty \frac{1}{N_{m-1}} \frac{1}{\sqrt{y_o a}} \left(\frac{y}{y_o a}\right)^{-1/3} e^{-y/(y_o a)} L_{m-1}^{-1/3} \cdot \sqrt{\frac{2}{\pi}} \begin{Bmatrix} \sin(\rho y) \\ \cos(\rho y) \end{Bmatrix} dy \tag{50}$$

where upper terms in brackets refer to LSE and lower to LSM polarization.

From [15] the solution of integral is found as

$$P_{m\rho} = \frac{1}{N_{m-1}} \sqrt{\frac{2a}{\pi y_o}} \frac{\Gamma(m - 1/3)}{(m-1)!} \frac{(\rho y_o a)^{m-1}}{[1 + (\rho y_o a)^2]^{(2m-1)/2}} \times \begin{Bmatrix} \sin \\ \cos \end{Bmatrix} [(m-1)\pi/2 + (m - 1/3) \cdot \operatorname{arctg}(\rho y_o a)]. \tag{51}$$

Same procedure as above is employed in order to get expressions for transformer coefficients of continuum mode of region II:

$$A_{m\rho} = \frac{1}{N_{m-1}} \sqrt{\frac{2a}{\pi y_o}} \frac{\Gamma(m - 1/3)}{(m-1)!} \frac{(\rho y_o a)^{m-1}}{[1 + (\rho y_o a)^2]^{(2m-1)/2}} \times \begin{Bmatrix} \sin[\alpha' + (m-1)\pi/2 + (m - 1/3) \cdot \operatorname{arctg}(\rho y_o a)] \\ \cos[\alpha'' + (m-1)\pi/2 + (m - 1/3) \cdot \operatorname{arctg}(\rho y_o a)] \end{Bmatrix}. \tag{52}$$

The transformer coefficients for discrete mode of region II integral given by (34) had to be solved. From [16] solution is found as

$$A_{mk} = \frac{1}{N_{m-1}} \sqrt{\frac{a}{y_o}} \begin{Bmatrix} A_s' \\ A_s'' \end{Bmatrix} \frac{\Gamma(m - 1/3)}{(m-1)!} \cdot \frac{\begin{Bmatrix} \gamma_k' \\ \gamma_k'' \end{Bmatrix}^{m-1} y_o a}{1 + \begin{Bmatrix} \gamma_k' \\ \gamma_k'' \end{Bmatrix}^{m-1/3} y_o a}. \tag{53}$$

References

[1] W. Zhou and T. Itoh, "Analysis of trapped image guides using effective dielectric constant and surface impedances," *IEEE Trans. Microwave Theory Tech.*, vol. MTT-30, pp. 2163–2166, Dec. 1982.

[2] D. D. King, "Properties of dielectric image lines," *IRE Trans. Microwave Theory Tech.*, vol. MTT-3, pp. 75–81, Mar. 1955.

[3] R. M. Knox and P. P. Toulios, "Integrated circuits for the millimeter through optical frequency range," in *Proc. Symp. Submillimeter Waves*, New York, 1970.

[4] S. Hedges and T. Rozzi, "The loss analysis of inset dielectric guide including bending loss and a comparison with image line," in *Proc. 17th European Microwave Conf.*, Rome, Sept. 1987, paper P4.5, pp. 933–938.

[5] T. Rozzi and L. Ma, "Mode completeness, normalization and Green's function of the inset dielectric guide," *IEEE Trans. Microwave Theory Tech.*, vol. 36, pp. 542–551, Mar. 1988.

[6] L. Ma, S. R. Pennock, and T. Rozzi, "Linear arrays realized in IDG," paper of the *IEE Coloquium Components for Novel Transmission Lines*, London, March 26, 1990, Dig. No. 1990/048.

[7] T. Rozzi and L. Ma, "An efficient mode launcher for arrays of longitudinal dipoles in IDG," in *IEEE MTT-S Int. Microwave Symp. Dig.*, 1990, paper MM6, pp. 1243–1246.

[8] T. Rozzi and S. Hedges, "Rigorous analysis and network modeling of the inset dielectric guide," *IEEE Trans. Microwave Theory Tech.*, vol. MTT-35, pp. 823–833, Sept. 1987.

[9] T. E. Rozzi, "Rigorous analysis of the step discontinuity in a planar dielectric waveguide," *IEEE Trans. Microwave Theory Tech.*, vol. MTT-26, pp. 738–746, Oct. 1978.

[10] T. Rozzi and G. In't Veld, "Field and network analysis of interacting step discontinuities in planar dielectric waveguides," *IEEE Trans. Microwave Theory Tech.*, vol. MTT-27, pp. 303–309, Apr. 1979.

[11] R. E. Collin, *Field Theory of Guided Waves*. New York: McGraw-Hill, 1960, p. 18.

[12] M. Abramovitz and I. A. Stegun. *Handbook of Mathematical Functions*. National Bureau of Standards, 1968, pp. 771–803.

[13] T. Rozzi, S. R. Pennock, and D. Boscovic, "Dispersion characteristic of coupled inset dielectric guide," in *Proc. 20th European Microwave Conf.*, Budapest, Sept. 1990, paper P1.20, pp. 1175–1180.

[14] T. Rozzi and J. S. Kot, "The complete spectrum of image line," *IEEE Trans. Microwave Theory Tech.*, vol. 37, pp. 868–876, May 1989.

[15] I. S. Gradshteyn and I. M. Ryshik, *Table of Integrals, Series and Products*. New York: Academic, 1965.
[16] A. Apelblat, *Table of Definite and Infinite Integrals*. Amsterdam: Elsevier, 1983.

Steve Pennock (M'88) was born in Birmingham, U.K., in 1959. He received the degree of B.Sc. in physics with electronics from the University of Liverpool, U.K., in 1980 and the degree of Ph.D. from the University of Bath, U.K., in 1986 for his work on the plasmatic control of dielectric waveguides.

From 1983 to 1985 he was a Research Assistant working on finline components for millimeter waves at the University of Bath, where, in 1985 he became a Lecturer. His current research interests include the modeling of uniform and nonuniform transmission structures, antennas, active and control circuits, and measurements, at microwave and millimeter wave frequencies.

Dragan M. Bošković (S'85–M'92) received the Dipl. Ing. and Magistar degrees, both in electrical engineering from the University of Belgrade, Yugoslavia, in 1983 and 1988 respectively, and the Ph.D. degree from the University of Bath, U.K., in 1991.

From 1983–1988 he was a Research Associate with the Institute of Applied Physics, Belgrade. He continued his career as a R&D engineer with Wessex Electronics, Bristol, U.K. In 1990 he joined the School of Electronic and Electrical Engineering, University of Bath as member of the research staff. His professional experience includes matching network synthesis for low noise and power amplifier designs, modeling nonlinear phenomena in microwave devices and use of numerical tools for study of electromagnetic problems, particularly dielectric guides.

Tullio Rozzi (M'66–SM'74–F'90), for a photograph and biography, see this issue, p. 1008.